Biosensors and Bioelectronics 285 (2025) 117583

Contents lists available at ScienceDirect

Biosensors and Bioelectronics

journal homepage: www.elsevier.com/locate/bios

Targeted molecular rapid SERS diagnosis in clinical human serum through aptamer origami-collapsed nanofingers chip

Beijia Ji [a,1], Zerui Liu [b,1], Zhekai Lv [a], Qihan Yang [a], Jingyi Sun [a], Guangxu Su [a], Yuxuan Xia [a], Xinxin Yan [a], Junzheng Hu [c], Pan Hu [b], Wanwan Yi [d], Chengyou Jia [d,*], Jiangbin Wu [e,**], Peng Zhan [c,***], Pingheng Tan [e], Wei Wu [b,****], Fanxin Liu [a,*****]

[a] School of Physics, Zhejiang University of Technology, Hangzhou, 310023, PR China
[b] Ming Hsieh Department of Electrical and Computer Engineering, University of Southern California, Los Angeles, CA, 90089, United States of America
[c] School of Physics, National Laboratory of Solid State Microstructures, Nanjing University, Nanjing, 210093, PR China
[d] Department of Nuclear Medicine, Shanghai Tenth People's Hospital, Tongji University, Shanghai, 200072, PR China
[e] State Key Laboratory of Superlattices and Microstructures Institute of Semiconductors, Chinese Academy of Sciences, Beijing, 100083, PR China

ARTICLE INFO

Keywords:
Aptamer
Origami
Collapsed nanofingers
Liquid serum
SERS

ABSTRACT

Surface-Enhanced Raman Scattering (SERS) offers great potential for label-free molecular diagnosis, especially in detecting disease biomarkers. However, the complexity of the biological environment in clinical human serum often significantly impairs detection accuracy. In this study, we present a highly effective SERS strategy utilizing aptamer origami-collapsed nanofingers for the precise qualitative and quantitative detection of specific targeted biomarkers in clinical serum. Here, the biomarker-specific aptamers are anchored to gold nanofingers, which then collapse during liquid evaporation, forming sub-nanometric gaps that enhance near-field strength. The serum is introduced directly into these stabilized nanofingers, where targeted biomarkers are selectively captured in aptamer hotspots, yielding pure Raman spectra of the biomarkers without interference from other serum molecules. The ratio of the biomarker's characteristic Raman peak to that of the aptamer allows for accurate quantification. This approach was validated with alpha-fetoprotein (AFP) for hepatocellular carcinoma and cardiac troponin I (cTnI) for acute myocardial infarction in clinical serum, achieving detection within 3 min. This strategy represents a significant advancement in SERS-based medical diagnostics, offering exceptional sensitivity and specificity in complex biological samples.

1. Introduction

Surface-Enhanced Raman Scattering (SERS) was widely thought to be a promising approach in disease identification because biomarkers can be directly fingerprinted through their Raman spectra (Shin et al., 2023; Wang et al., 2023; Schlücker and Choi, 2024; Wu and Qu, 2015; Seth et al., 2024). The plasmonic dimers with sub-nanometer scale gaps can create a coupled electromagnetic (EM) enhancement up to 10^3 fold which enables the Raman cross-section compared with that of fluorescence, resulting in highly sensitive detection down to single-molecular SERS detection (Xu et al., 1999; Nordlander et al., 2004; Savage et al., 2012; Moskovits, 2013; Baumberg et al., 2019; Le Ru and Auguié, 2024). In addition, SERS can provide a fast assay and real-time monitoring for biomarkers up to several seconds, and requires a tiny amount of samples (Graham et al., 2017; Langer et al., 2020; Lin et al., 2021; Ma et al., 2024). These capabilities of SERS hold significant potential for advancing medical diagnosis (Schlücker and Choi, 2024). Usually, target biomarkers associated with different diseases remain in

* Corresponding authors.
** Corresponding authors.
*** Corresponding authors.
**** Corresponding author.
***** Corresponding author.
E-mail addresses: jiachengyou@tongji.edu.cn (C. Jia), jbwu@semi.ac.cn (J. Wu), zhanpeng@nju.edu.cn (P. Zhan), wu.w@usc.edu (W. Wu), liufanxin@zjut.edu.cn (F. Liu).
[1] B. J. and Z. L. contributed equally to this work.

https://doi.org/10.1016/j.bios.2025.117583
Received 9 February 2025; Received in revised form 17 April 2025; Accepted 12 May 2025
Available online 13 May 2025

clinical blood for a prolonged period, and thus, the serum is selected as a sample in modern medical diagnosis (Seth et al., 2024). However, when serum is directly used as samples in SERS for the ground truth measurement (Yu et al., 2020), both the qualitative and quantitative biomarkers detection still face challenges that limit its applications in medical diagnosis (Lee et al., 2024a). As is well known, in qualitative SERS analysis for biomarkers in serum, besides biomarkers, there are over thousands of diverse molecules and direct measurement using serum will form a mixture of Raman spectra, so the specific biomarkers cannot be directly identified (Shi et al., 2023). Further, in quantitative SERS analysis, multiple factors, including uncontrollable molecular absorption or desorption in hotspots, heterogeneous SERS enhancement, and optical operations, induce notable Raman signal intensity fluctuations, which produce larger errors in quantification (Zhang et al., 2023).

The strategies to overcome these limitations based on plasmonic dimers nanostructures have been broadly introduced. The first strategy employing bottom-up self-assembly methods is that versatile plasmonic dimer metallic colloidal nanoparticles by DNA assisted technology have been designed in solution, making known pure small molecules be embedded just inside the DNA cavity where the EM field reaches the maximum value (Cao et al., 2002; Cheng et al., 2017; Hilal et al., 2022; Lee et al., 2024b; Lee et al., 2024c; Yang and Lim, 2020; Yeşilyurt et al., 2023; Schuknecht et al., 2023; Liu et al., 2023a). However, these approaches are basically not practical for the biomarkers because the target biomarkers in serum are difficult to be selectively trapped into the DNA cavity. The second strategy employing top-down etching methods is that different dimer solid chips have been fabricated in which the gap sizes are currently limited to several nanometers (Le Ru and Auguié, 2024; Ma et al., 2024; Shvalya Abdulhalim et al., 2020; Shrivastav et al., 2024; Singh et al., 2023). The main difficulty is that present solid chips require the sample purification process to avoid the formation of a mixture spectra but are impractical for clinical serum (Ma et al., 2024).

In this work, we propose that by combining the flexible Au nanofingers solid chip with aptamer origami-assisted technology, specific biomarkers in clinical serum can be exclusively captured in highly uniform hotspots of aptamer gaps between pairs of nanofingers, achieving a fully pure SERS spectrum only including biomarkers and aptamer without the disturbance of other molecules so that the qualitative analysis can be achieved. In addition, this sub-nanometer aptamer gap can provide a highly enhanced near field so that SERS detection can reach up to single-molecule level. Furthermore, a uniform single-layer of aptamers on the Au nanofingers can be selected as the internal standard, and the Raman intensities ratio of specific biomarkers to aptamer enables highly accurate quantification. As proof of concepts, both a specific biomarker of alpha-fetoprotein (AFP) for hepatocellular carcinoma (HCC) (Zhu et al., 2019), and the cardiac biomarker of cardiac troponin I (cTnI) for acute myocardial infarction (AMI) (Lee et al., 2024d), were successfully demonstrated in serum. The strategy significantly expedites the practical applications of SERS in medical molecular diagnosis.

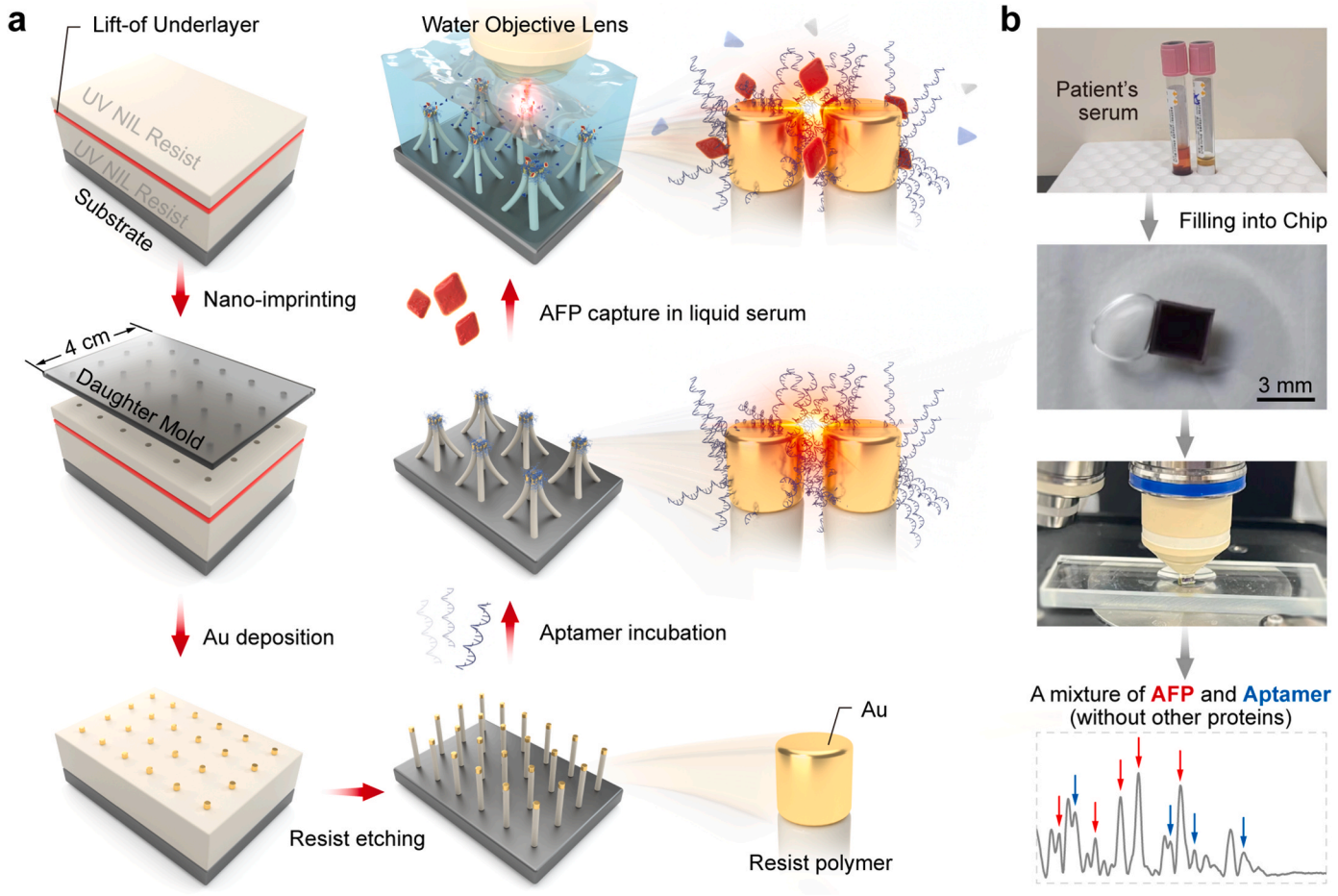

Fig. 1. Schematic strategy for biomarkers' SERS detection in clinical serum. (a) First, flexible nanofingers are fabricated by NIL. Then, Au nanofingers are incubated in an AFP-aptamer solution. Finally, a collapsible process induces gap plasmons between pairs of nanofingers. In SERS measurement, the liquid serum is directly filled into the chip and AFP is uniquely captured in hotspots by aptamers which are detected by a water lens. **(b)** Clinical serum is filled into the chip. As a result, a mixture of the Raman spectra of AFP and aptamers is acquired.

2. Materials and methods

The flexible Au nanofingers were fabricated by the well-developed nanoimprint lithography (NIL) (Hu et al., 2010; Song et al., 2017; Liu et al., 2018). The fabrication procedure of flexible Au nanofingers is described schematically in Fig. 1. First, UV-curable NIL was utilized to transfer the original hole pattern to a polymeric reverse-tone (pillar) daughter mold. Then subsequent NIL, residual layer etching, metal evaporation, and lift-off steps were performed to create an Au caps array. As the pattern can be defined precisely by the initial interference lithography and duplicated reliably by NIL, an array of nanofingers can be fabricated uniformly over a large area with high throughput after etching the uncovered UV nanoimprint resist. To form ordered quadramer-like nanofinger collapsing with the polarization independence, the aspect ratio of fingers is well controlled to ~4 because high aspect ratio will result in a random collapse with a large number of fingers. The incubation process of aptamers on Au nanofingers was shown in the supporting materials. The current clinical trial was performed from April 2021 to August 2024 by the Third Affiliated Hospital of Naval Medical University, which was approved by the institutional review board of Shanghai No. 10 People's Hospital (SHSY-IEC-5.0/23K31/P01). The criteria for enrollment for HCC and AMI patients were shown in the supporting materials. The concentration of certain substances in each patient was conducted following the gold standard method as shown in the supporting materials.

3. Results and discussion

The strategy for specific biomarkers' SERS detection in clinical serum is schematically shown in Fig. 1, in which AFP is first selected as a proof of concept (Zhu et al., 2019). It is noted here that the use of Au nanofingers is mainly attributed to their good chemical stability and biological activity. These fabricated nanofingers are incubated in an aptamer solution in which the aptamers are pre-connected to the Au surface via thiol-binding (Zhao et al., 2019; Li et al., 2018). During the air-drying process, Au disks on top of flexible nanofingers physically touch each other driven by capillary force (Lee et al., 2024d). Au/aptamers/Au gap plasmonic structures are consequently achieved in which double-layer aptamers are used as the spacer layer between pairs of nanofingers (Su et al., 2023; Li et al., 2007). Au/aptamers/Au nanofingers are pre-stabilized at the bottom of the biocarrier glass-slide, which forms a solid SERS chip. When serum is directly filled into this chip, AFP can be exclusively captured in hotspots between aptamers' origami-collapsed nanofingers (Fig. 1a). Using a water objective lens finely focusing on the surface of nanofingers, only captured AFP near hotspots can be directly detected, thereby avoiding the disturbance from other molecules. Finally, a mixture of AFP and aptamer Raman signals is acquired (Fig. 1b). Through the identification of AFP-characterized Raman bands, AFP can be exclusively detected.

The SEM images of Au nanofingers indicate that the diameter of nanofingers and lattice spacing are 70 nm and 130 nm, respectively, as shown in Fig. 2a & b. HR-TEM further demonstrates the successful formation of the collapsed Au/aptamers/Au structure (Fig. 2e). The height of nanofingers is 300 nm including 250 nm polymer support and 50 nm Au disks on top (Fig. 2e). The measured transmittance spectra indicate that a localized surface plasmon resonance (LSPR) centered at approximately 650 nm for un-collapsed nanofingers can be observed, which is ascribed to a plasmon-induced dipole resonance of a single Au nanofinger (Fig. 2c). After collapsing, this LSPR has a significant redshift to 750 nm (Fig. 2c), which is ascribed to the stronger near-field interactions of the two collapsed Au nanofingers (Lee et al., 2006; Li et al., 2016). In addition, the simulations were performed using COMSOL Multiphysics, in which the model matched the experimental observation. The permittivity of Au is interpolated from the experimental data (Johnson and Christy, 1972), and the refractive index of the polymer is set as 1.41 (Liu et al., 2018). The incident EM field was polarized along the dimer axis. As shown in Fig. 2d, the LSPR of Au nanofingers showed a redshift from 650 nm to 750 nm before and after collapse (Liu et al., 2018), which was consistent with the experiment. The EM field of collapsed nanofingers under 785 nm excitation, which is the Raman excitation wavelength, showed that the strongest EM field would reach up to thousands times of the incident field at the nanoscale gap region (Fig. 2f). It is widely acknowledged that the SERS enhancement factor is proportional to the fourth power of the local EM field enhancement

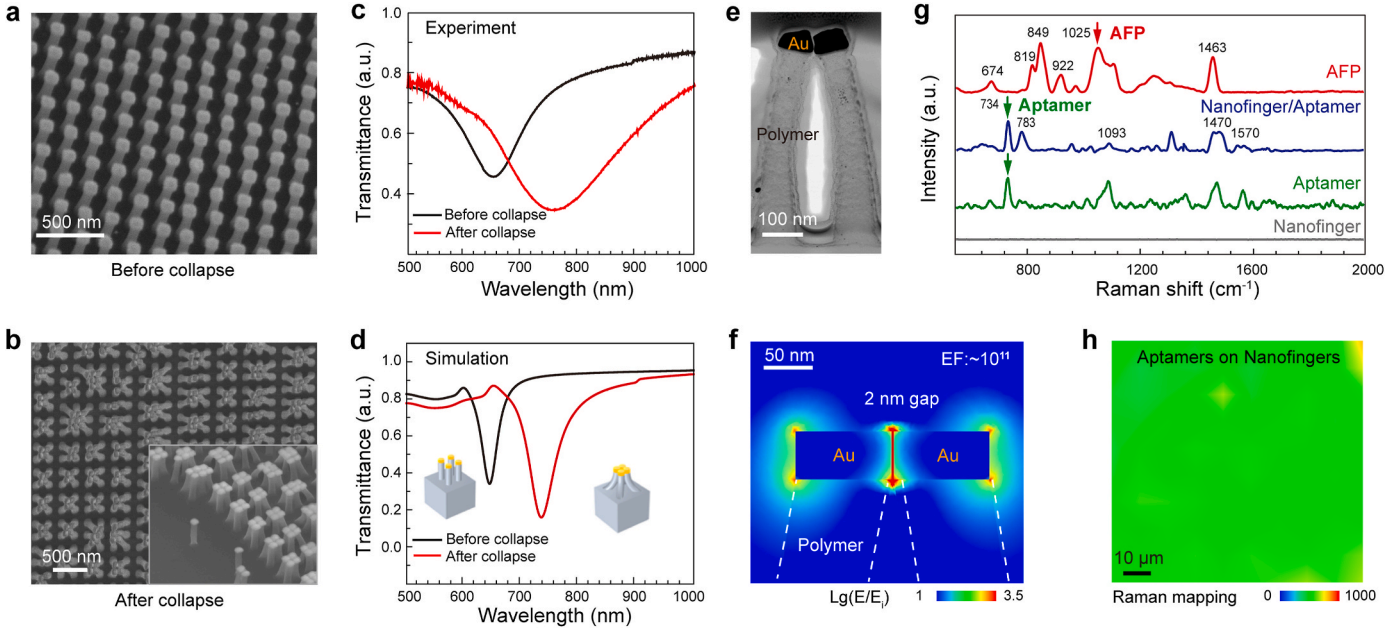

Fig. 2. Characterizations for aptamer origami-collapsed Au-nanofingers. SEM images of nanofingers before collapse (**a**) and after collapse **(b)**. **(c) & (d)** Experimental and calculated transmittance spectra. **(e)** HR-TEM cross-sectional-view of collapsed Au-nanofingers. **(f)** Cross-sectional distribution of calculated EM field at 785 nm excitation. **(g)** Standard Raman spectra of pure AFP, pure aptamer, aptamer/Au-nanofingers, and Au nanofingers, respectively. **(h)** Raman mapping at 734 cm^{-1} for aptamer/Au-nanofingers.

((E/E_{inc}) (Wu and Qu, 2015)) (Moskovits, 2013). In this case, the resultant SERS enhancement factor is ~1 × 10^{11}, which enables the single-molecule SERS detection.

To demonstrate the effectiveness of this strategy, standard Raman spectra of pure AFP, pure aptamer and aptamer/Au-nanofingers were first acquired, as shown in Fig. 2g. The results indicate that pure aptamer shows characteristic peaks centered at 734 cm^{-1} (adenine, A), 783 cm^{-1} (cytosine, C), 1093 cm^{-1} (P-O), 1470 cm^{-1} (C-H) and 1570 cm^{-1} (C=C) (Barhoumi et al., 2008). Aptamer/Au-nanofingers have shown characteristic peaks at 734 cm^{-1}, 783 cm^{-1}, 1093 cm^{-1}, 1470 cm^{-1} and 1570 cm^{-1} which still mostly remain consistent with pure aptamer, and a little difference can be ascribed to the chemical agent of Tris-EDTA (TE) solvent because the Au nanofingers show no Raman signals. Thus, the characteristic Raman peaks of aptamer/Au-nanofingers are used as a standard in later analysis. The Raman spectra of pure AFP are mainly centered at 674 cm^{-1}, 819 cm^{-1}, 849 cm^{-1}, 1025 cm^{-1} (phenylalanine), and 1463 cm^{-1} (C-H) (Er et al., 2021). The significant difference between aptamer's and AFP's Raman fingerprints, which can serve to indicate the existence of AFP, makes them highly distinguishable. Typical Raman peaks at 734 cm^{-1} for aptamer and at 1025 cm^{-1} for AFP are selected for later mapping analysis. The mapping was performed for aptamer/Au-nanofingers in which the relative standard deviation of the intensity data was ~11.5 %, showing good uniformity (Fig. 2h). Though there are some inevitable defects of nanofinger array, the use of the intensity ratio of AFP to aptamer can greatly decrease the errors in quantification analysis.

The aptamer/Au-nanofingers were first used to detect pure AFP solution with concentrations ranging from 0.001 ng/mL to 10 ng/mL. The criterion of detection sensitivity for AFP in hospital is 1 ng/mL. The Raman mapping with a step of 10 μm was performed over a square region of 100 μm × 100 μm in which 785 nm excitation with 3 mW incident power was used, and the collection time for a single spectrum was 0.5 s. Time-resolved dynamic Raman mappings were monitored at 2-min intervals. As expected, as time interval gets longer, the detected counts of AFP will increase, as schematically shown in Fig. 3a. As shown in Fig. 3c, the dynamic Raman mappings for 0.01 ng/mL AFP basically confirm that the detected counts and Raman intensity of AFP at the same spots marked by dotted circles increase over a longer time interval by the continuous capture. Through extracting Raman spectra in dotted circles, AFP intensity at 1025 cm^{-1} increases over the time interval, which proves that the aptamers can continuously capture AFP into the hotspots in the liquid, as shown in Fig. 3b. However, the Raman intensity of the captured AFP at some position has fluctuations at the same spots with the time interval, which can be ascribed to molecules'

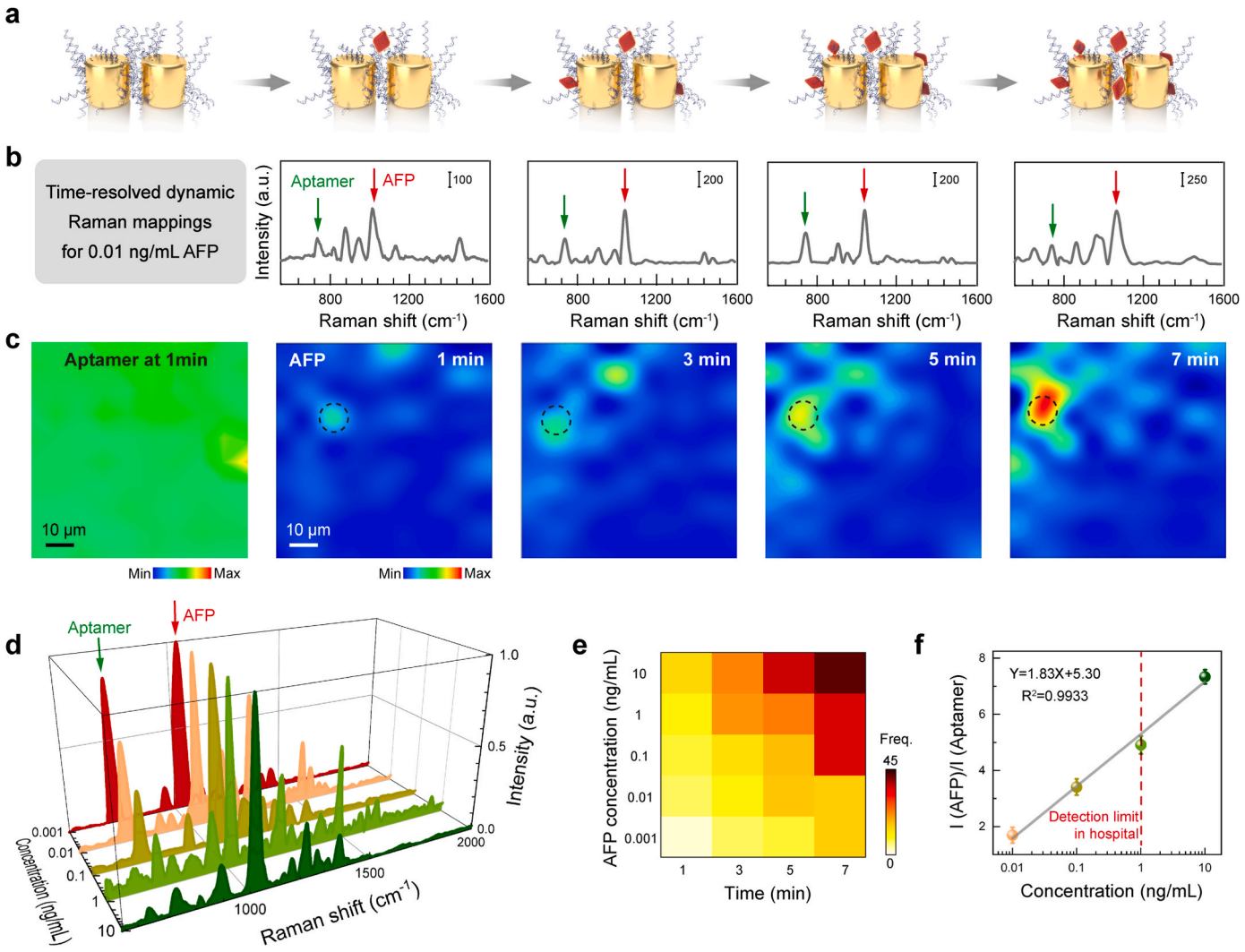

Fig. 3. Pure AFP solutions Raman measurements. (a) Schematic of AFP dynamic capture in solution. **(b)** Raman spectra extracted from the mappings circled with black dotted lines in (c). **(c)** Dynamic Raman mappings for AFP solution with 0.01 ng/mL. **(d)** Respective Raman spectra at 5 min for different concentrations. **(e)** The counts of captured AFP vary with different AFP concentrations. **(f)** The ratio I (AFP)/I (Aptamer) varies with AFP concentrations ranging from 10 ng/mL to 0.01 ng/mL.

absorption or desorption in the liquid, and thermal effect by incident laser (Zhang et al., 2023). The results of other AFP concentrations (Fig. S1 in supporting materials) indicate the same observation.

Furthermore, the Raman intensity and the counts of captured AFP molecules also increase with the increase of concentrations at the same time interval (Fig. 3c and Fig. S1), which can be used for quantification. But the aptamer Raman signals at 734 cm^{-1}nearly remain unchanged with different AFP concentrations (Fig. 3c and Fig. S2). Thus, the ratio of Raman intensity of AFP to aptamer can be used to accurately quantify AFP so that optical fluctuation can be avoided. Considering that the absorption or desorption of AFP over time intervals induces the change of its Raman intensity at the same position, the average of I_{AFP} (1025 cm^{-1}) divided by the average of $I_{Aptamer}$ (734 cm^{-1}) can be a readout to predict the concentration of AFP. Here, Raman mapping spectra at 5-min intervals are selected for analysis, mainly because AFP at this time instant can be obviously captured with enough detected counts (Fig. 3e). The respective Raman spectra for different AFP concentrations at 5-min are shown in Fig. 3d. The recorded $I_{AFP}/I_{Aptamer}$ with AFP concentrations ranging from 10 ng/mL to 0.01 ng/mL are shown in Fig. 3f. The results indicate a nearly linear relation $y = 1.83x + 5.30$ with $R^2 = 0.9933$ between $I_{AFP}/I_{Aptamer}$ (y) and AFP concentration (x). For the ultralow concentration of 0.001 ng/mL, there are few captured counts and the statistical average is not accurate for predicting the ultralow concentrations by present mappings.

To prove effectiveness in medical diagnosis, clinical liquid serum samples were further tested. The patient's information was shown in Table S1 and AFP was pre-determined by the gold standard method (supporting materials). Time-resolved dynamic Raman mappings for AFP in the patient's serum (21 ng/mL) and healthy serum are shown in Fig. 4b & c. The results clearly indicate that there is hardly any signal of the AFP molecules in healthy serum even with a 5-min interval, while AFP can be easily captured even at a 1-min interval in patient's serum. This is mainly attributed to the fact that the concentration of AFP molecules in healthy serum is extremely low so that only very tiny AFP molecules can be possibly captured by the aptamers after such a short time interval. At the same spots as dotted circles shown in Fig. 4b, AFP Raman signals show an increase from 1 min to 3 min and then keep stable from 3 min to 5 min, as proved by the extracted typical Raman spectra shown in Fig. 4a. It may be ascribed to a high concentration in which large amounts of AFP are easily captured and become saturated in a short time interval.

To further illustrate the exclusive capture of AFP by aptamer in liquid serum, the Raman spectra of pure AFP and AFP in patient's serum are integrated for clear comparison, as shown in Fig. 4d. The results indicate that the Raman spectrum for clinical serum is not a mixture of other proteins and only includes the AFP (819 cm^{-1}, 930 cm^{-1}, 1025 cm^{-1}, 1465 cm^{-1}) and aptamer (734 cm^{-1}, 1093 cm^{-1}, 1465 cm^{-1}) signals which can be characterized by standard Raman spectra of pure AFP and aptamer/Au-nanofingers. However, when the serum was dripped directly onto the surface of the nanofingers and air dried, numerous Raman peaks appeared which could be ascribed to a mixture of Raman spectra containing over thousands of other molecules in serum, preventing direct fingerprint Raman detection for specific biomarkers in serum (Liu et al., 2023b; Leong et al., 2023; Kim et al., 2024). If the samples are washed, the Raman spectra may become clear, but they cannot be used for quantification because it is not a ground truth measurement. Therefore, our strategy provides a highly effective detection for specific biomarkers in a complex clinical serum.

To further demonstrate accurate quantification in patient's serum, the ratio of the average I_{AFP} (1025 cm^{-1}) and $I_{Aptamer}$ (734 cm^{-1}) is used as a readout to predict the concentration of AFP. The Raman spectra at 3-min intervals are selected for quantification because AFP with different concentrations can be obviously captured and the respective Raman spectra are shown in Fig. 4e. The results indicate a good linear relation with $R^2 = 0.9987$ between I_{1025}/I_{734} and AFP concentration in clinical serum, and the slope of the correlation line is 2.52, as shown in Fig. 4f. By comparing the linear equations of $y = 1.83x + 5.30$ (for pure AFP) and $y = 2.52x + 0.88$ (for AFP in serum), the difference can be ascribed to the solvents used in which the solvents in clinical serum are more complex. Nevertheless, the relative error between them is only 27 % ((2.52–1.83)/2.52) which is acceptable in the application of in vitro diagnostic (IVD) products.

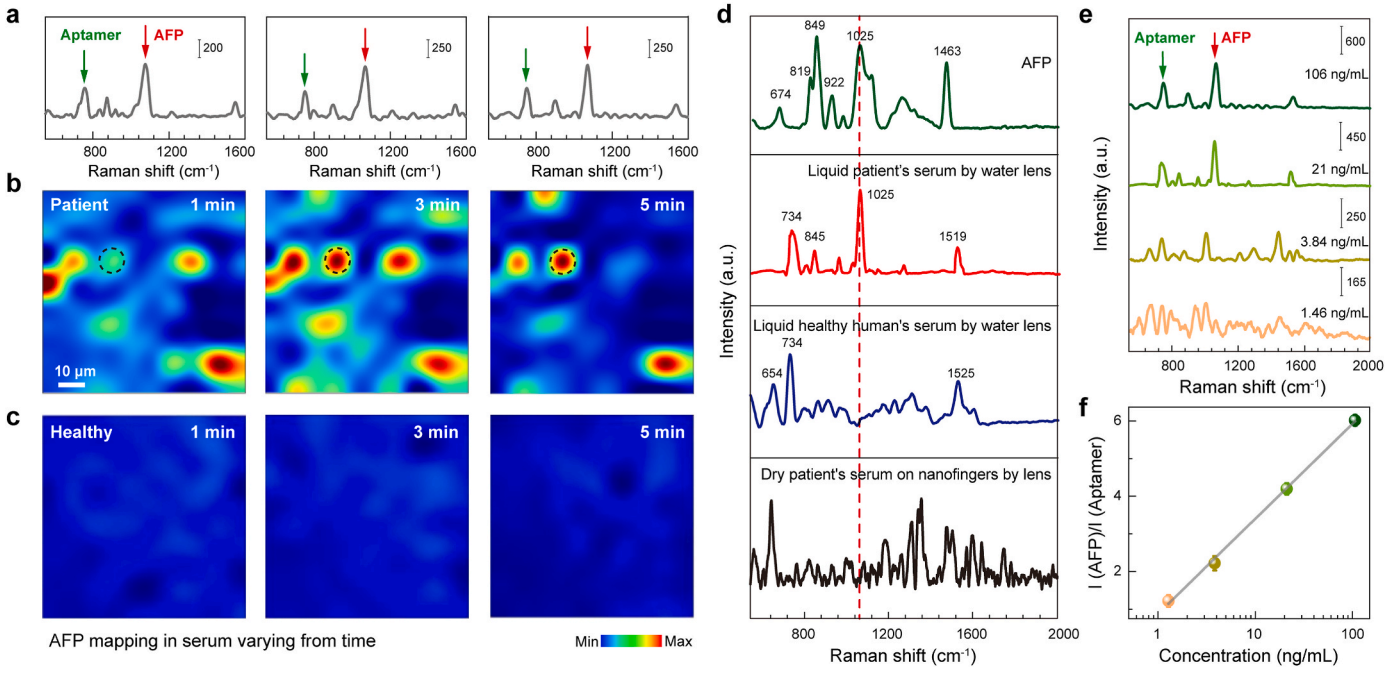

Fig. 4. AFP Raman detection in serum. (a) Raman spectra extracted from areas circled with black dotted lines in (b). **(b)** Dynamic Raman mappings for patient's serum (21 ng/mL) and **(c)** for healthy serum. **(d)** Raman spectra of pure AFP, patient's liquid serum and healthy serum by water lens, and dried patient's serum on nanofingers by normal lens. **(e)** Respective Raman spectra at 3 min for different AFP concentrations in serum. **(f)** The I (AFP)/I (Aptamer) ratio of AFP varies with different AFP concentrations in the patient's serum.

The above results successfully demonstrated the detection of specific biomarkers in serum within 3 min which is very helpful for a time-critical and high-risk disease, for example, acute myocardial infarction (AMI) with high mortality worldwide. cTnI molecule is one of the most important biomarkers for AMI. Here, the cTnI-aptamer Raman signals at 740 cm^{-1} nearly remain unchanged with time interval (Fig. 5a). Time-resolved dynamic Raman mappings for cTnI at 1060 cm^{-1} in clinical patient's serum (6.796 ng/mL) and healthy serum are shown in Fig. 5b & c. The results indicate that cTnI in serum can be easily captured even at 1-min intervals, which is much shorter than that by immunofluorescence (~12 min in hospitals). In addition, as shown in Fig. 5d, the Raman spectrum of patient's serum by suggested strategy is not a mixture and only includes both cTnI (852 cm^{-1}, 913 cm^{-1}, 1060 cm^{-1}, 1125 cm^{-1}, 1480 cm^{-1}) and aptamer (740 cm^{-1}, 852 cm^{-1}, 913 cm^{-1}, 1480 cm^{-1}). All results, including both AFP and cTnI measurements, demonstrate the robustness and high accuracy of the suggested method, highlighting its potential as a reliable diagnostic tool that can be integrated into clinical workflows for prompt and accurate medical diagnosis.

4. Conclusions

In summary, this study demonstrated an effective SERS platform for the detection of specific biomarkers in a patient's serum with accurate qualitative and quantitative analysis. Through the pre-connection between aptamer and Au surface, the flexible Au nanofingers then collapse onto each other to form aptamer origami-collapsed nanofingers. Liquid serum is directly filled into nanofingers and the biomarkers can be uniquely captured without any disturbance from other molecules in a complex clinical serum within 3 min. In addition, the ratio of biomarkers' Raman intensity to aptamer can provide high accuracy for quantification. This strategy indicates promising potential for SERS applications in a broad range of antigen–aptamer reactions for biomarkers detection in clinical serum, and it can enable SERS in practical medical diagnosis.

CRediT authorship contribution statement

Beijia Ji: Validation, Methodology, Investigation, Formal analysis, Data curation. **Zerui Liu:** Validation, Methodology, Investigation, Formal analysis, Data curation. **Zhekai Lv:** Investigation, Data curation. **Qihan Yang:** Investigation, Data curation. **Jingyi Sun:** Investigation, Data curation. **Guangxu Su:** Methodology, Funding acquisition. **Yuxuan Xia:** Data curation. **Xinxin Yan:** Data curation. **Junzheng Hu:** Data curation. **Pan Hu:** Data curation. **Wanwan Yi:** Data curation. **Chengyou Jia:** Methodology, Funding acquisition. **Jiangbin Wu:** Writing – review & editing, Supervision. **Peng Zhan:** Supervision, Funding acquisition. **Pingheng Tan:** Supervision. **Wei Wu:** Supervision, Resources, Project administration. **Fanxin Liu:** Writing – review & editing, Writing – original draft, Supervision, Resources, Project administration, Methodology, Funding acquisition, Conceptualization.

Declaration of competing interest

I, [Fanxin Liu], representing all authors, declare that there are there are no conflicts of interest in relation to the manuscript titled "Targeted Molecular Rapid SERS Diagnosis in Human Serum Through Aptamer Origami-Collapsed Nanofingers Chips" submitted to *Biosensors and Bioelectronics*. I, representing all authors, confirm that the results and interpretations reported in the manuscript are original and have not

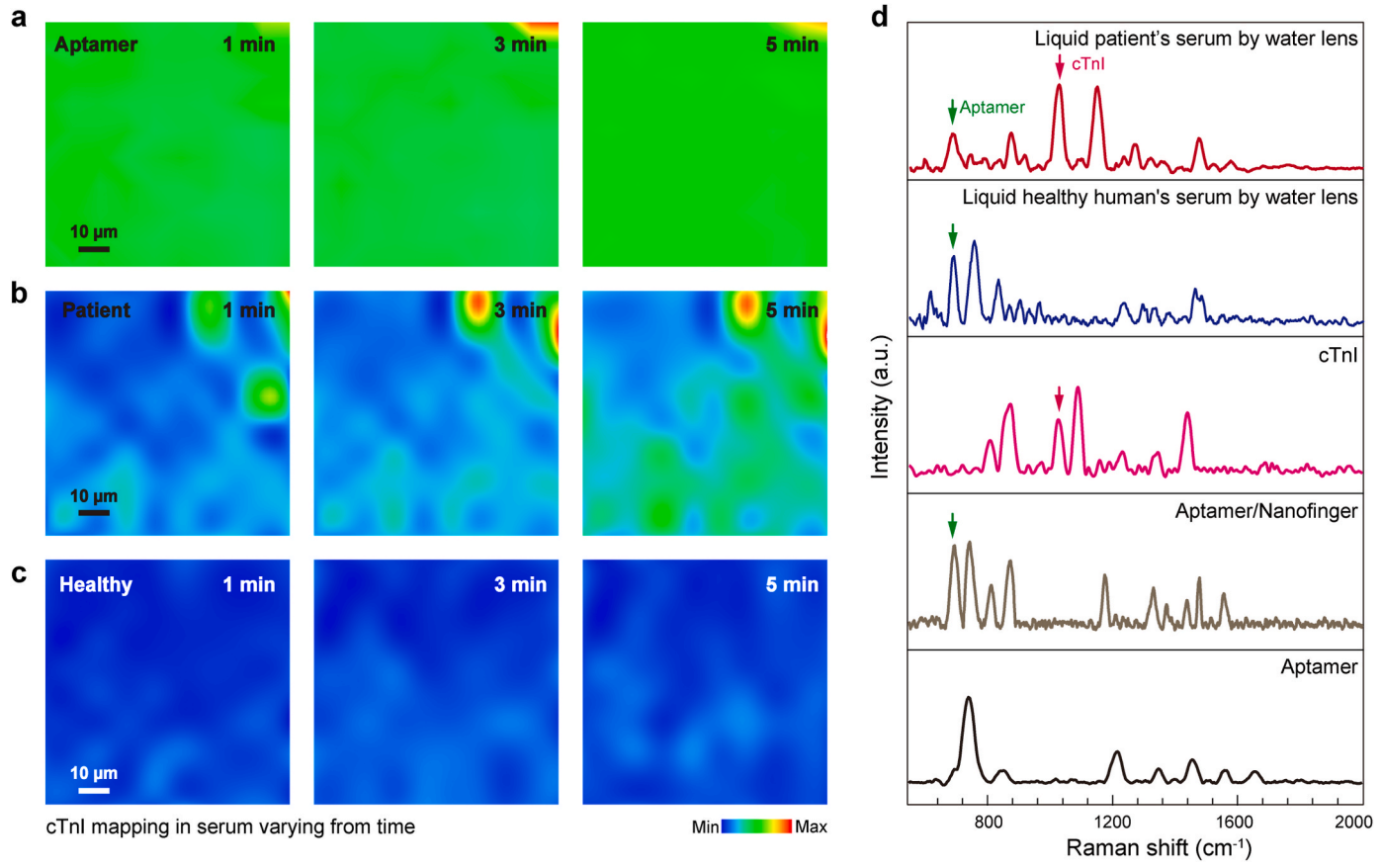

Fig. 5. cTnI Raman detection in serum. Dynamic Raman mappings for aptamer **(a)**, for cTnI in AMI serum with 6.796 ng/mL **(b)** and in healthy serum **(c)**. **(d)** Raman spectra of AMI serum at 3 min, healthy serum at 3 min, pure cTnI, aptamer/Au-nanofingers, and pure aptamer.

been plagiarized.

I, representing all authors, certify that I have read and understand the *Biosensors and Bioelectronics* conflict of interest policy, and I understand that the failure to disclose a conflict of interest may result in the manuscript being rejected or retracted.

I, representing all authors, also certify that I have disclosed any financial or non-financial relationships that may be interpreted as constituting a conflict of interest in relation to this manuscript. In understand that this information will be subject to peer review, and I am willing to provide further information or clarification if required.

I, representing all authors, confirm that I have no known conflicts of interest that would influence the results or interpretation of the data presented in this manuscript, and I understand that failure to disclose a conflict of interest is unethical and may result in sanctions being imposed on me.

Acknowledgement

This work was supported by National Natural Science Foundation of China (Nos. 11974015, 12174189, and 12304431), Natural Science Foundation of Zhejiang Province (No. LZ22A040008), and National Key R&D Program of China (No. 2022YFA1404300). This work is partially supported by the project of Shanghai Municipal Health Commission (202040043; GWVI-11.2-YQ51 and 20214Y0159).

Appendix A. Supplementary data

Supplementary data to this article can be found online at https://doi.org/10.1016/j.bios.2025.117583.

Data availability

Data will be made available on request.

References

Barhoumi, A., Zhang, D.M., Tam, F., Halas, N.J., 2008. J. Am. Chem. Soc. 130, 5523–5529.
Baumberg, J.J., Aizpurua, J., Mikkelsen, M.H., Smith, David R., 2019. Nat. Mater. 18, 668–678.
Cao, Y.C., Jin, R., Mirkin, C.A., 2002. Science 297, 1536–1540.
Cheng, Z., Choi, N., Wang, R., Lee, S., Moon, K.C., Yoon, S.-Y., Chen, L., Choo, J., 2017. ACS Nano 11, 4926–4933.
Er, E., Sánchez-Iglesias, A., Silvestri, A., Arnaiz, B., Liz-Marzán, L.M., Prato, M., Criado, A., 2021. ACS Appl. Mater. Interfaces 13, 8823–8831.
Graham, D., Moskovits, M., Tian, Z.Q., 2017. Chem. Soc. Rev. 46, 3864–3865.
Hilal, H., Zhao, Q., Kim, J., Lee, S., Haddadnezhad, M., Yoo, S., Lee, S., Park, W., Park, W., Lee, J., Lee, J.W., Jung, I., Park, S., 2022. Nat. Commun. 13, 4813.
Hu, M., Ou, F.S., Wu, W., Naumov, I., Li, X.M., Bratkovsky, A.M., Williams, R.S., Li, Z.Y., 2010. J. Am. Chem. Soc. 132, 12820–12822.
Johnson, P.B., Christy, R.W., 1972. Phys. Rev. B 6, 4370.
Kim, J.Y., Koh, E.H., Yang, J.Y., Mun, C., Lee, S.H., Lee, H.Y., Kim, J.W., Park, S.G., Kang, M.J., Kim, D.H., Jung, H.S., 2024. Adv. Funct. Mater. 34, 2307584.
Langer, J., de Aberasturi, D.J., Aizpurua, J., Alvarez-Puebla, Ramon A., Auguie, B., 2020. ACS Nano 14, 28–117.
Le Ru, Eric C., Auguié, B., 2024. ACS Nano 18, 9773–9783.
Lee, S.J., Morrill, A.R., Moskovits, M., 2006. J. Am. Chem. Soc. 128, 2200–2201.
Lee, S.W., Dang, H.J., Moon, J., Kim, K.Y., Joung, Y.J., Park, S.Y., Yu, Q., Chen, J.D., Lu, M.D., Chen, L.X., Joo, S.-W., Choo, J., 2024a. Chem. Soc. Rev. 53, 5394–5427.
Lee, S., Kwon, S., Lee, S., Oh, M., Jung, I., Park, S., 2024b. Nano Lett. 24, 3930–3936.
Lee, S., Lee, S., Park, W., Lee, S., Kwon, S., Oh, Myeong J., Haddadnezhad, M.N., Jung, I., Kim, B., Park, J., Shin, K.S., Lee, H., Yoo, J., Kim, W.-K., Park, S., 2024c. Nano Lett. 24, 4233–4240.
Lee, H., Kim, W., Song, M.-Y., Kim, D.-H., Jung, H.S., Kim, W., Choi, S.J., 2024d. Small 20, 2304999.
Leong, S.X., Tan, Emily X., Han, X.M., Luhung, I., Aung, N.W., Nguyen, L.B.T., Tan, S.Y., Li, H.T., 2023. In: Phang, Y., Schuster, S., Ling, X.Y. (Eds.), ACS Nano, vol. 17, pp. 23132–23143.
Li, D., Shlyahovsky, B., Elbaz, J., Willner, I., 2007. J. Am. Chem. Soc. 129, 5804–5805.
Li, A.R., Srivastava, S.K., Abdulhalim, I., et al., 2016. Nanoscale 8, 15658–15664.
Li, G.Y., Li, S.S., Wang, Z.H., Xue, Y.W., Dong, C.Y., Zeng, J.X., Huang, Y., Liang, J.T., Zhou, Z.D., 2018. Anal. Biochem. 547, 37–44.
Lin, D., Hsieh, C.L., Hsu, K.C., Liao, P.H., Qiu, S.F., Gong, T.X., Yong, K.T., Feng, S.Y., Kong, K.V., 2021. Nat. Commun. 12, 3430.
Liu, F.X., Song, B.X., Su, G.X., Liang, O., Zhan, P., Wang, H., Wu, W., Xie, Y.H., Wang, Z. L., 2018. Small 14, 1801146.
Liu, Y.N., Zeng, T., Liu, C., Fang, X., Li, S.Q., Cao, X.P., Lu, C.H., Yang, H.H., 2023a. Nano Lett. 23, 11569–11577.
Liu, Z.R., Meng, D.M., X Su, G., Hu, P., Song, B.X., Wang, Y.X., Wei, J.H., Yang, H., Yuan, T.Y., Chen, B.Y., Ou, T.H., Hossain, S., Miller, M., Liu, F.X., Wu, W., 2023b. Small 19, 2204719.
Ma, H., Pan, S.Q., Wang, W.L., Yue, X.X., Xi, X.H., Yan, S., Wu, D.Y., Wang, X., Liu, G.K., Ren, B., 2024. ACS Nano 18, 14000–14019.
Moskovits, M., 2013. Phys. Chem. Chem. Phys. 15, 5301–5311.
Nordlander, P., Oubre, C., Prodan, E., Li, K., Stockman, M.I., 2004. Nano Lett. 4, 899–903.
Savage, K.J., Hawkeye, M.M., Esteban, R., Borisov, A.G., Aizpurua, J., Baumberg, J.J., 2012. Nature 491, 574–577.
Schlücker, S., Choi, N., 2024. ACS Nano 18, 5998–6007.
Schuknecht, F., Kołątaj, K., Steinberger, M., Lied, T., Lohmueller, T., 2023. Nat. Commun. 14, 7192.
Seth, A., X Liu, Y., Gupta, R., Wang, Z.Y., Mittal, E., Kolla, S., Rathi, P., Gupta, P., Parikh, B.A., Genin, G.M., Gandra, S., Storch, G.A., Philips, J.A., George, I.A., Singamaneni, S., 2024. Nano Lett. 24, 229–237.
Shi, L.Y., Li, Y.J., Li, Z., 2023. Light Sci. Appl. 12, 234.
Shin, H., Choi, B.H., Shim, O., Kim, J., Park, Y., Cho, S.K., Kim, H.K., Choi, Y., 2023. Nat. Commun. 14, 1644.
Shrivastav, A.M., Abutoama, M., Abdulhalim, I., 2024. Nanoscale Adv. 6, 5681–5693.
Shvalya, V., Abdulhalim, I., et al., 2020. Appl. Phys. Rev. 7, 031307.
Singh, N., Shrivastav, A.M., Vashistha, N., Abdulhalim, I., 2023. S. ensors & Actuators: Biol. Chem. 374, 132813.
Song, B.X., Yao, Y.H., Groenewald, R.E., Wang, Y.X., Liu, H., Wang, Y.F., Li, Y.R., Liu, F. X., Cronin, S.B., Schwartzberg, A.M., Cabrini, S., Hass, S., Wu, W., 2017. ACS Nano 11, 5836–5843.
Su, G.X., Hu, P., Hu, J.Z., Wang, X.L., Wu, G.L., Shang, Y.P., Zhan, P., Liu, F.X., Wu, W., 2023. J. Raman Spectrosc. 54, 6–12.
Wang, Y.M., Fang, L.R., Wang, Y.H., Xiong, Z.Z., 2023. Adv. Sci., 2300668
Wu, L., Qu, X.G., 2015. Chem. Soc. Rev. 44, 2963–2997.
Xu, H.X., Bjerneld, E.J., Kall, M., Borjesson, L., 1999. Phys. Rev. Lett. 83, 4357.
Yang, W., Lim, D.W., 2020. Adv. Mater. 32, 2002219.
Yeşilyurt, A.T.M., Wu, X.F., Tapio, K., Bald, I., Huang, J.S., 2023. J. Am. Chem. Soc. 145, 25928–25932.
Yu, Y., Xiao, T.H., Wu, Y.Z., Li, W.J., Zeng, Q.G., Long, L., Li, Z.Y., 2020. Adv. Photo. 2, 014002.
Zhang, R.Y., Li, L.W., Guo, Y., Shi, Y.F., Li, J.F., Long, Y.T., Fang, J.X., 2023. Nano Lett. 23, 11771–11777.
Zhao, J., Wu, C., Zhai, L.P., Shi, X.F., Li, X., Weng, G.J., Zhu, J., Li, J., Zhao, J.W., 2019. J. Mater. Chem. C 7, 8432–8441.
Zhu, A.N., Zhao, X.Y., Cheng, M.Y., Chen, L., Wang, Y.X., Zhang, X.L., Zhang, Y.J., Zhang, X.F., 2019. ACS Appl. Mater. Interfaces 11, 44617–44623.